Tri- and Diglycine Backbone Rotational Dynamics Investigated by ^{13}C NMR Multiplet Relaxation and Molecular Dynamics Simulations†

Vladimir A. Daragan‡ and Kevin H. Mayo*

Department of Biochemistry, Biomedical Engineering Center, University of Minnesota Health Sciences Center, 420 Delaware Street, Southeast, Minneapolis, Minnesota 55455

Received June 29, 1993; Revised Manuscript Received August 19, 1993®

ABSTRACT: Backbone motional dynamics in tri- and diglycine have been investigated by using ^{13}C NMR multiplet relaxation spectroscopy. Dipolar auto- and cross-correlation times were determined as a function of pH, ionic strength, and temperature. Molecular dynamics simulations and φ,ψ bond rotation energy profiles were calculated for insight into the physical nature of backbone rotations that could contribute to ^{13}C relaxation. Various motional models were used to fit the experimental data. For internal glycine G2 in triglycine, restricted and unrestricted rotational diffusion models both underestimate internal correlation times, although they do agree that the axis of fastest internal rotation is directed closely along the C_α–C bond. For di- and triglycine, significant pH dependencies in cross-correlation times for C-terminal glycines, and more so for those of N-terminal glycines, indicate the importance of the ionization state in internal mobility of terminal backbone positions. For terminal glycines, rotational jump models which allow for diffusive-like fluctuations within minima best explain the experimental data. φ,ψ rotational fluctuation amplitudes and internal rotational energy barriers derived from the temperature dependence of ^{13}C relaxation parameters, which range from 3 to 5 kcal/mol, agree well with those values calculated in rotational energy profiles.

The problem of adequately describing peptide backbone rotational dynamics by NMR[1] relaxation normally concerns limited experimental data and the choice of an appropriate mathematical model. Models currently used for analysis of NMR relaxation data include those which describe anisotropic unrestricted diffusion, multiple rotations, restricted diffusion [see, for example, a review by London (1980)], and wobbling-in-a-cone motions (Lipari & Szabo, 1980, 1981). Various model-free approaches (Ribeiro et al., 1980; Lipari & Szabo, 1982a,b; Clore et al., 1990a,b) for obtaining non-physically-related information about rotational correlation times and characteristics of restricted motions in terms of order parameters are also available. With limited experimental data, it is often difficult to choose which model is best, and the simplest model that can describe all available experimental parameters is then normally chosen. To date, the model-free approach has been used most often. This may be fine for qualitative correlation with NMR/NOE structural analyses, but it falls short in more detailed descriptions of peptide/protein dynamics.

With the development of genetic cloning techniques and rapid peptide synthesis, the concern over data limitation and accuracy has waned, and a new dimension has been opened to the study of peptide/protein dynamics by using NMR relaxation methods. Generation of more accurate experimental data has led to a renaissance in the development of motional models and NMR relaxation data. For example, two-dimensional ^{15}N relaxation experiments performed at different frequencies (Clore et al., 1990a,b) have shown the necessity of introducing an additional internal correlation time into the Lipari and Szabo (1982a,b) model-free approach. ^{13}C NMR multiplet relaxation in peptides has shown the need to include a geometric term in the theoretical analysis and a limitation in simple model-free approaches in describing the sign of the dipolar cross-correlation function (Daragan & Mayo, 1993). Daragan et al. (1993a) have shown that a model of restricted diffusion best describes ^{13}C NMR multiplet relaxation data on a hexadecapeptide. Even this model, however, could not describe adequately the temperature dependence of the dipolar cross-correlation function. A possible explanation for this concerns the importance of fast rotational fluctuations within rotational energy minima.

In the present article, simple peptides, i.e., Gly-Gly and Gly-Gly-Gly, allow a rather complete analysis of backbone motions from ^{13}C NMR relaxation data. Data collected at different temperatures, pH's, and ionic strengths are obtained from analysis of auto- and cross-correlation times (Daragan et al., 1974; Werbelow & Grant, 1975, 1977; Bain & Lynden-Bell, 1975). Cross-correlation terms provide useful information about the anisotropy of rotational motions (Daragan & Mayo, 1992). Various models of peptide internal rotations have been related to calculated rotational energy profiles and molecular dynamics simulations. Here it will be shown how fast rotational fluctuations within rotational energy minima can be introduced into an analysis of auto- and cross-correlation times.

In addition, the influences of pH and ionic strength have been investigated to address the role of electrostatic interactions in backbone rotational dynamics. Of the few papers written on this subject, Saitô and Smith (1974) have found, by using proton-decoupled ^{13}C relaxation on pure lysine and glycine monomers, that the rotational correlation times for motions of C_α–H vectors plateau at the zwitterionic state. At high or low pH, correlation times increase more than 100% for glycine

† This work was supported by a National Research Council/National Science Foundation International (USSR) Project Development grant to K.H.M. and benefited from NMR facilities made available through Grant RR-04040 from the National Institutes of Health.

* Corresponding author.

‡ On leave from the Institute of Chemical Physics, Russian Academy of Sciences, 117977, Moscow, Russia.

® Abstract published in *Advance ACS Abstracts,* October 15, 1993.

[1] Abbreviations: NMR, nuclear magnetic resonance; rf, radio frequency; GGG, triglycine; GG, diglycine.

0006-2960/93/0432-11488$04.00/0

and about 25% for lysine. The zwitterionic form apparently has the greatest degree of rotational mobility. On the other hand, no difference in the correlation times of C_α–H vectors in the tripeptide, $(Lys)_3$, was observed. For penta-L-lysine, only a small decrease in the C_α–H correlation time was seen for the N-terminal residue at high pH. It is interesting to note that for tri-L-lysine correlation times of C_β–H vectors also decreased at high pH. In another work, Saitô and Smith (1973) measured spin-lattice relaxation times for the dodecapeptide, $(Lys)_{12}$, and for poly-L-lysine (MW = 2850). No pH dependence was observed, except for increases in all correlation times at pH >10.5, where a coil–helix transition occurs. For a collagenous 16-residue peptide, Daragan et al. (1993b) found that, at low pH, internal mobility increases, especially for the N-terminal glycine.

THEORY

General Equations. For inversion–recovery experiments (Daragan et al., 1974; Bain & Lynden-Bell, 1975), the equations for initial relaxation rates for inner (W_i) and outer (W_o, average value for left and right) lines of the $^{13}CH_2$ NMR multiplet spectrum can be written as

$$W_i = W_{CH} + W_{CSA} - W_{HCH}$$
$$W_o = W_{CH} + W_{CSA} + W_{HCH} \quad (1)$$

where

$$W_{CH} = 2h^2\gamma_C^2\gamma_H^2 J^*_{CH}/r_{CH}^6$$
$$W_{HCH} = 0.6h^2\gamma_C^2\gamma_H^2 J_{HCH}(\omega_C)/r_{CH}^6 \quad (2)$$

h is Planck's constant divided by 2π, r_{CH} is the internuclear distance between carbon and its bonded hydrogen, and γ_C and γ_H are the magnetogyric ratios for the carbon and hydrogen nuclei, respectively. W_{CSA} is the contribution to relaxation from the chemical shift anisotropy. This term is small in the case of triglycine and later will be neglected (Daragan & Mayo, 1993).

$$J^*_{CH}(\omega_C) = {}^3/_{10}[{}^1/_3 J_{CH}(\omega_H - \omega_C) + J_{CH}(\omega_C) + 2J_{CH}(\omega_C + \omega_H)] \quad (3)$$

where ω_C and ω_H are the ^{13}C and ^1H resonance frequencies, respectively, in radians/s, and $J_{CH}(\omega)$ and $J_{HCH}(\omega_C)$ are the auto- and cross-correlation dipolar spectral densities, respectively:

$$J_{CH}(\omega) = 4\pi\int_0^\infty Y_{20}(\theta_{CH}(t))Y_{20}(\theta_{CH}(0))\cos\omega t\,dt$$
$$J_{HCH}(\omega) = 4\pi\int_0^\infty Y_{20}(\theta_{CH'}(t))Y_{20}(\theta_{CH}(0))\cos\omega t\,dt \quad (4)$$

where Y_{20} is the second-rank spherical harmonic. θ_{CH} is the angle between the CH vector and, for example, the direction of the static magnetic field.

For triglycine, the nuclear Overhauser coefficient for ^{13}C–$\{^1H\}$ is equal to its maximum value, indicating that the extreme narrowing limit has been reached. Spectral densities are now related directly to auto- and cross-correlation times as

$$\tau_{CH} = J_{CH}{}^*(0) \quad \text{and} \quad \tau_{HCH} = J_{HCH}(0) \quad (5)$$

For many models describing molecular rotations, the general expression for the dipolar spectral density function can be written as (Daragan & Mayo, 1993)

$$J_{ab}(\omega) = a^0_{ab}F_0(\omega) + a^1_{ab}F_1(\omega) + a^2_{ab}F_2(\omega) \quad (6)$$

where **a** and **b** are vectors directed along interacting nuclei. For **a** = **b**, we have the autocorrelation spectral density, and in the case of **a** ≠ **b**, we have the cross-correlation spectral density. Auto- and cross-correlation times can be defined as $\tau_{ab} = J_{ab}(0)$. a^0_{ab}, a^1_{ab}, and a^2_{ab} are coefficients which depend on the CH_2 group geometry and orientation of internal rotation axes. If the molecular frame z-axis is directed along the axis of internal rotation, then

$$a^0_{ab} = 0.25(3\cos^2\theta_a - 1)(3\cos^2\theta_b - 1)$$
$$a^1_{ab} = 3\cos\theta_a\cos\theta_b\sin\theta_a\sin\theta_b\cos(\phi_a - \phi_b) \quad (7)$$
$$a^2_{ab} = ({}^3/_4)\sin^2\theta_a\sin^2\theta_b\cos 2(\phi_a - \phi_b)$$

where θ_a, θ_b, ϕ_a, and ϕ_b are the polar angles of the **a** and **b** vectors in the molecular frame. For tetrahedral geometry of the methylene group, one can write

$$\tau_{CH} = {}^1/_9F_0(0) + {}^8/_{27}F_1(0) + {}^{16}/_{27}F_2(0) \quad (8)$$
$$\tau_{HCH} = {}^1/_9F_0(0) - {}^4/_{27}F_1(0) - {}^8/_{27}F_2(0)$$

It is obvious from eq 8 that $\tau_o = F_0(0) = 3(\tau_{CH} + 2\tau_{HCH})$ is the correlation time of the z-axis tumbling. The functions $F_0(\omega)$, $F_1(\omega)$, and $F_2(\omega)$ depend on the particular molecular motion model being used. For isotropic reorientation with correlation time $\tau_o = F_0(0)$ and z-axis internal rotation angle $\gamma(t)$,

$$F_m(\omega) = \int_0^\infty \exp(-t/\tau_o)\,\Phi_m(t)\cos\omega t\,dt \quad (9)$$

where $\Phi_m(t)$ is the correlation function of internal rotation:

$$\Phi_m(t) = \langle\exp(m_i(\gamma(t_o + t)) - \gamma(t_o))\rangle \quad (10)$$

If z-axis rotational motion is not isotropic, but can be described by symmetric top rotational diffusion (Huntrees, 1968), then

$$F_m(\omega) = \int_0^\infty\Phi_m(t)\sum_{m_1=0}^{2}B_{m1,m}(\beta)\exp(-t(6D_{xx} + m_1{}^2)(D_{zz} - D_{xx}))\cos\omega t\,dt \quad (11)$$

where

$$B_{m_1,m}(\beta) = [d^2{}_{m_1,m}(\beta)]^2 + [d^2{}_{m_1,m}(\beta)]^2 \qquad m_1 \neq 0$$
$$B_{0},m(\beta) = [d^2{}_{0,m}(\beta)]^2 \quad (12)$$

Here, $d^2{}_{m_1,m}(\beta)$ is a function derived from factorization of the second-order Wigner rotation matrix. β is the angle between the z-axis of the molecular coordinate system and the z-axis of the rotational frame, where the rotational diffusion tensor is diagonalized with the main values D_{zz} and $D_{xx} = D_{yy}$. For two independent rotations (Wallach, 1967),

$$F_m(\omega) = \int_0^\infty\Phi_m(t)\sum_{m_1,m_2=0}^{2}B_{m_2,m_1}(\beta)B_{m_1,m}(\beta_1)\times\Phi_{m_2}(t)\,F_{overall}(t)\cos\omega t\,dt \quad (13)$$

where β_1 is the angle between internal rotation axes, $\Phi_{m_2}(t)$ and $\Phi_m(t)$ are correlation functions of the first and second internal rotations with respect to the rotational diffusion tensor frame, for example, and $F_{overall}(t)$ is the correlation function of overall molecular tumbling.

Random Walks within Potential Wells. Here, rotational fluctuations are determined as rotationally restricted motions in a potential well(s). Numerous approaches exist to solve

this problem, e.g., restricted rotational diffusion in rectangular wells with reflecting boundary conditions (Witterbort & Szabo, 1978; London & Avitable, 1978), rotational diffusion in the potential well (the Smoluchowski equation) (Edholm & Blomberg, 1979), Sack's equation, where inertial effects are taken into account (Sack, 1957; Zatsepin, 1977), as well as consideration of general properties of correlation functions for such motions (Newman, 1982). In order to solve this problem analytically and to significantly simplify analysis, a simple model which considers rotational motion in a potential well where inertial effects are ignored is used to describe the influence of such motions on NMR relaxation.

Consider time-dependent rotations through an angle $\gamma(t)$ in a potential well $U(\gamma)$. Rotations are considered to be rotational jumps between defined states: $\gamma_0 = 0$, $\gamma_{\pm1} = \pm\gamma_1$, $\gamma_{\pm2} = \pm\gamma_2$, with an equal potential energy difference between states. For the sake of simplicity, consider three states, −1, 0, and +1, where 0 is the state at the bottom of the well, and potential energy differences are $U_{+1} - U_0 = U_{-1} - U_0 = \Delta E$. Transition probabilities between the nearest points can be defined as $W^+ = W(+1,0) = W(-1,0)$ and $W^- = W(0,+1) = W(0,-1)$.

The probability of finding the system in some state can be written by kinetic equations:

$$\begin{aligned} dP_0/dt &= W^-(P_{-1} + P_{+1}) - 2W^+P_0 \\ dP_{-1}/dt &= W^+P_0 - W^-P_{-1} \\ dP_1/dt &= W^+P_0 - W^-P_1 \end{aligned} \tag{14}$$

At equilibrium,

$$P_1/P_0 = P_{-1}/P_0 = W^+/W^- = \exp(-\Delta E/RT) \tag{15}$$

where R is the molar gas constant. The probabilities, P_i, are conditional upon

$$\sum_{i=-1}^{1} P_i = 1 \tag{16}$$

The linear differential equations (14) have been solved (Tsutsumi, 1979). Equation A2.1 of (Tsutsumi (1979) has been misprinted. Any correlation function related with $\gamma(t)$ can be written as

$$CF(t) = \langle F(\gamma(t_0 + t),\gamma(t_0))\rangle = \sum_{i,j=-n}^{n} F(\gamma_i,\gamma_j)P(i,t/j)P_i \tag{17}$$

where γ_i,γ_j are the angles which correspond to the i and j states and P_i are the *a priori* probabilities of finding orientational state i and obey eqs 15 and 16. $P(i,t/j)$ is the conditional probability of finding state i after a time t if there was initially a state j.

Let us define

$$W = W^- + 2W^+ \tag{18}$$

After the kinetic equations are solved, one can write correlation functions

$$\Gamma(t) = \langle\gamma(t_0 + t)\gamma(t_0)\rangle = 2(W^+/W)\gamma_1^2 \exp(-W^-t)$$

and

$$\begin{aligned} \Phi_m(t) = \langle\exp(-m_i[\gamma(t_0 + t) - \gamma(t_0)])\rangle = (W^-/W + \\ 2(W^+/W)\cos(m\gamma_1))^2 + 2(W^+W^-/W^2)(1 - \cos(m\gamma_1))^2 \\ \exp(-Wt) + 2(W^+/W)\sin^2(m\gamma_1)\exp(-W^+t) \end{aligned} \tag{19}$$

If $W^+/W^- = \exp(-\Delta E/RT) \ll 1$, then $\Phi_m(t)$ in eq 19 can be simplified to

$$\Phi_m(t) = 1 - 4(W^+/W^-)(1 - \cos(m\gamma_1))(1 - \exp(-W^+t)) \tag{20}$$

For practical purposes, one can neglect the exponential term in eq 20, since the decay of the total rotational correlation function is usually much shorter than other types of rotational motions in peptides. Therefore, for the simple model of overall molecular isotropic reorientation with internal rotational fluctuations in some potential well, one can write the total correlation function as

$$\begin{aligned} \Phi_m^{tot}(t) = \Phi_m(t)\exp(-t/\tau_0) = (1 - C_m^f + C_m^f\exp(-W^+t)) \times \\ \exp(-t/\tau_0) \\ \approx (1 - C_m^f)\exp(-t/\tau_0) \end{aligned} \tag{21}$$

where

$$C_m^f = 4\exp(-\Delta U(\gamma_1)/RT)(1 - \cos(m\gamma_1)) \tag{22}$$

The influence of eq 17 on the actual correlation function will be determined later after the energetic rotational profiles for triglycine are calculated.

Rotational Jump Models. First consider the simplest case: rotational jumps between two minima separated by an angle 2γ and located at $+\gamma_1$ and $-\gamma_1$. In this case, the kinetic equations have the form:

$$\begin{aligned} dP^+/dt &= W(P^+ - P^-) \\ dP^-/dt &= -W(P^+ - P^-) \end{aligned} \tag{23}$$

By using formulas from the previous section, one can calculate the correlation functions

$$\Gamma(t) = \langle\gamma(t_0 + t)\gamma(t_0)\rangle = \gamma_1^2\exp(-2Wt)$$

and

$$\begin{aligned} \Phi_m(t) = \langle\exp(-m_i[\gamma(t_0 + t) - \gamma(t_0)])\rangle = \\ \cos^2(m\gamma_1) + \sin^2(m\gamma_1)\exp(-2Wt) \end{aligned} \tag{24}$$

If one considers a three-state jump model where the central minimum is located at $\gamma = 0$ and the positions of the two small minima are located at $+\gamma$ and $-\gamma$, then the transition probabilities W_0 and W_1 define transitions from the central to the outer (W_0) and from the outer to the central (W_1) minima. The kinetic equations for this model are similar to those given in eq 14. When $W_0 \ll W_1$, the correlation functions can be written as:

$$\Gamma(t) = 2(W_0/W_1)\gamma^2\exp(-W_1t)$$

and

$$\Phi_m(t) = 1 - 4(W_0/W_1)(1 - \cos(m\gamma))(1 - \exp(-W_1t)) \tag{25}$$

Calculation of Correlation Times. First, it should be noted that, for all models mentioned above, a simplified equation for the correlation function of internal rotations can be written as:

$$\Phi_m(t) = (1 - C_m) + C_m\exp(-t/\tau_i) \tag{26}$$

where τ_i is the correlation time of internal rotation. For the three-state jump model and for the simple random walk model within a potential well, the expression for C_m is given by equation 22. For the two-state jump model, $C_m = \sin^2(m\gamma)$. For the model of restricted rotational diffusion (London & Avitable, 1978) with angular limits $(-\gamma,\gamma)$ and correlation

time $\tau_i = 4\gamma^2/(\pi^2 D_i)$, where D_i is the diffusion coefficient for internal motion, one can write:

$$\Phi_0(t) = 1$$

and

$$\Phi_m(t) = \sum_{n=0}^{\infty} \Gamma_m^n(\gamma) \exp(-n^2 t/\tau_i) \qquad m = 1, 2 \qquad (27)$$

where

$$\Gamma_m^0(\gamma) = \sin^2(m\gamma)/(m^2\gamma^2)$$

and for $n > 0$,

$$\Gamma_m^n(\gamma) = m^2\gamma^2[\cos^2(m\gamma)\,(1 - (-1)^n) + \sin^2(m\gamma)\,(1 + (-1)^n)]/[(m^2\gamma^2) - (n\pi/2)^2]^2$$

With reasonable accuracy, one can write eq 27 in the form of eq 26 with $C_m = 1 - \sin^2(m\gamma)/(m\gamma)^2$.

Let us consider the equations that describe the dipolar auto- and cross-correlation times. If one considers isotropic reorientation of the molecular frame z-axis and only one internal rotation, then from eq 8 one can write expressions for the cross- and autocorrelation times as

$$\tau_{CH} = (1 - 2C(\gamma))\tau_o + 2C(\gamma)\tau_o\tau_i/(\tau_o + \tau_i) \qquad (28a)$$

and

$$\tau_{HCH} = (-^1/_3 + C(\gamma))\tau_o - C(\gamma)\tau_o\tau_i/(\tau_o + \tau_i) \qquad (28b)$$

where

$$C(\gamma) = {}^4/_{27}(C_1 + 2C_2) \qquad (29)$$

In the eq 28a the autocorrelation time τ_{CH} is similar to that found in the Lipari and Szabo model-free approach (Lipari & Szabo, 1982a,b), with order parameter $S^2 = 1 - 2C(\gamma)$. Here, it must be noted that eq 28 contains geometric characteristics of the methylene group and the orientation of the CH vector in the molecular frame. Therefore, from eqs 7, 9, and 26, for example, one can write an expression for the autocorrelation time τ_{HH}, which describes intramolecular dipolar proton relaxation, and an expression for the cross-correlation time τ_{CHH}, which can be derived from heteronuclear NMR relaxation experiments. For tetrahedral geometry of the CH_2 group,

$$\tau_{HH} = (1 - {}^3/_4 C_2)\tau_o + {}^3/_4 C_2\tau_o\tau_i/(\tau_o + \tau_i) \qquad (30a)$$

and

$$\tau_{CHH} = ({}^1/_2 - {}^1/_3 C_2)\tau_o + {}^1/_3 C_2\tau_o\tau_i/(\tau_o + \tau_i) \qquad (30b)$$

One can see that the Lipari and Szabo order parameter for τ_{HH} autocorrelation times is equal to $S^2 = 1 - {}^3/_4 C_2$. However, for cross-correlation times, the equations become quite complex and cannot be described by the Lipari and Szabo approach.

Since $C(\gamma)$ is rather important for interpreting our experimental data, this function is expressed below for different models of internal rotation:

model of two-state rotational jumps:

$$C(\gamma) = ({}^4/_{27}) \sin^2\gamma\,(1 + 8\cos^2\gamma) \qquad (31a)$$

model of three-state rotational jumps:

$$C(\gamma) = ({}^{16}/_{27})(W_o/W_1)(3 - \cos\gamma - 2\cos 2\gamma) \qquad (31b)$$

model of restricted rotational diffusion:

$$C(\gamma) = ({}^4/_9)(1 - \sin^2\gamma/(3\gamma^2)(1 + 2\cos^2\gamma)) \qquad (31c)$$

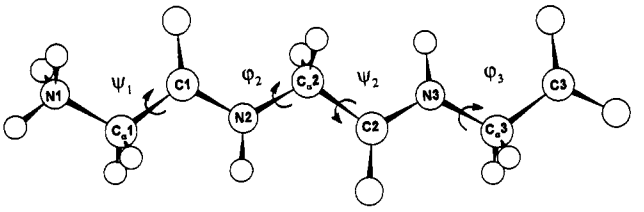

FIGURE 1: Illustrated triglycine backbone with labeled dihedral angles, as discussed in the text.

model of random walks within a parabolic potential

$$U(\gamma) = k\gamma^2$$

$$C(\gamma) = ({}^{16}/_{27}) \exp(-k\gamma^2/RT)\,(3 - \cos\gamma - 2\cos 2\gamma) \qquad (31d)$$

MATERIALS AND METHODS

Peptide Synthesis. $^{13}C_\alpha$-enriched tri- and diglycine were synthesized on a Milligen/Millipore automatic peptide synthesizer Excell by using standard Fmoc-BOP solid-phase chemistry (Atherton & Sheppard, 1989). Fmoc-[$^{13}C_\alpha$]glycine was prepared from [$^{13}C_\alpha$]glycine (CIL, Cambridge) and Fmoc-OSu (Calibochem). Peptides were cleaved from the resin by reagent R (trifluoroacetic acid/thioanisole/ethanedithiol/anisol, 90:5:3:3, v/v/v/v) for 2 h. Crude peptides obtained from TFA solution by precipitation with cold ethyl ether were purified by preparative HPLC on a C18 wide-pore column (Vydac) by elution in the water phase. The purity of prepared peptides was checked by analytical HPLC in the same solvent system on a C18 Bondclone (Phenomenex) column. Peptide concentration was determined from the dry weight of freeze-dried samples.

Nonisotopically enriched tri- and diglycine were purchased from Sigma Co. and were used without further purification. Purity (>95%) was checked by proton and carbon NMR spectroscopy.

NMR Spectroscopy. All measurements were performed on a Bruker AMX-600 NMR spectrometer at ^{13}C frequencies of 150 MHz. The temperature was varied from 278 to 348 K. Spin-lattice relaxation was studied by the homonuclear inversion–recovery method. The number of acquisitions was chosen to give a signal to noise ratio greater than 6. Therefore, the number of transients varied from 32 to 256. Ten to fifteen time-incremented (partially relaxed) spectra were routinely acquired for each relaxation measurement. To reduce errors from rf field inhomogeneities, the composite 180° pulse, $90°_x$–$180°_y$–$90°_x$, was used. To minimize the error in determining initial relaxation rates, a least-squares method with weighted functions has been used (Daragan et al., 1993a).

NOE measurements were made by using the gated decoupling pulse sequence with a time delay of more than 10 spin-lattice relaxation times (Canet, 1976). NOE coefficients represent an average of five separate measurements performed for each temperature. Statistical errors were less than about 5%.

Freeze-dried samples for NMR measurements were dissolved in D_2O. Peptide concentrations ranged from 3.5 to 25 mg/mL. pH was adjusted by adding microliter quantities of NaOD or DCl. Initially, no additional salts were added to the solution.

RESULTS

For ease in following the ensuing analysis, Figure 1 illustrates the triglycine backbone with rotation angles and C/N atoms labeled as discussed in the text.

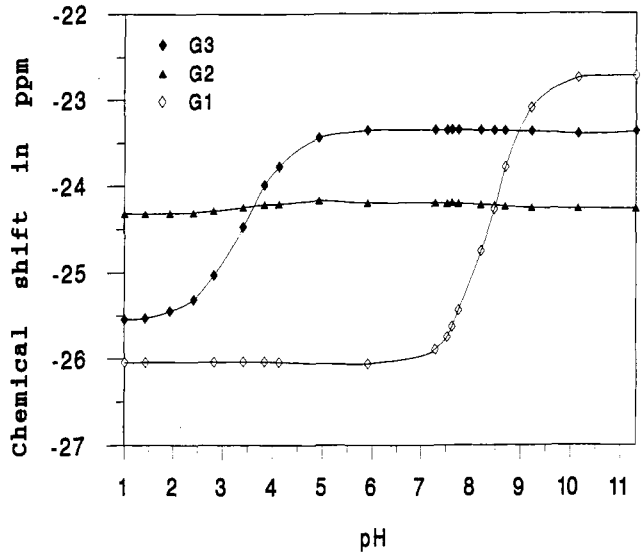

FIGURE 2: Titration curves for carbon-13 chemical shifts of the methylene groups in triglycine at 303 K. Peptide concentration is 10 mg/mL.

^{13}C NMR Data. The pH dependence of $^{13}C_\alpha$ chemical shifts in triglycine is shown in Figure 2. G1, G2, and G3 are clearly distinguished by their respective pH dependencies. The Henderson–Hasselbalch equation yields pK_a's for G1 and G3 of 3.4 and 8.4, respectively. Interestingly, G1 and G3 also demonstrate small chemical shift inflections at each others' pK_a values. The zwitterionic form of triglycine exists between pH 5 and 7. Below pH 2.5, the C-terminal carboxylate is protonated, leaving only the N-terminus charged (positive), and above pH 9.5 the N-terminal amine is deprotonated, leaving only the C-terminus charged (negative). G2 shows much smaller chemical shift inflections at these pK_a values.

Initially, spin-lattice relaxation times were derived from proton-decoupled inversion–recovery experiments on non-^{13}C-enriched triglycine. Autocorrelation times τ_{CH} were calculated by using eq 5, and their values at 303 K are plotted in Figure 3 as a function of solution pH. Only τ_{CH} for G1 and G3 exhibits significant pH dependencies consistent with the G1 and G3 pK_a values. τ_{CH} for G3 is sensitive to pH variations below pH 5, while τ_{CH} for G1 is most sensitive above pH 7. Interestingly, τ_{CH} for G1 even shows some pH sensitivity below pH 4, in an apparent reflection of the C-terminal carboxylate titration. With respect to the zwitterionic form of triglycine, τ_{CH} values at low pH indicate increased rotational mobility for G1 and decreased rotational mobility for G3. At higher pH values, only G1 displays increased mobility; G2 and G3 remain relatively unaffected.

For a more detailed analysis of backbone internal mobilities in triglycine, the temperature dependencies (278–348 K) of autocorrelation, τ_{CH}, and cross-correlation, τ_{HCH}, times derived from ^{13}C multiplet relaxation experiments have been acquired at pH values of 2.2, 5.6, and 10.7. For increased sensitivity and resolution of inner and outer multiplet lines, these ^{13}C relaxation measurements have been made on triglycine selectively enriched in ^{13}C, one glycine at at time: $^{13}G_1G_2G_3$, $G_1{}^{13}G_2G_3$, and $G_1G_2{}^{13}G_3$. The results are shown in Figures 4 and 5. Apparent linearity in plots of log τ_{CH} versus inverse temperature (K^{-1}) (Figure 4) justifies use of the Arrhenius equation in analyzing the temperature dependence of autocorrelation times. Least-squares fits to these plots yield activation energies, E_{CH}, as given in Table I. For all glycines, E_{CH} values increase with increasing pH. The most pronounced

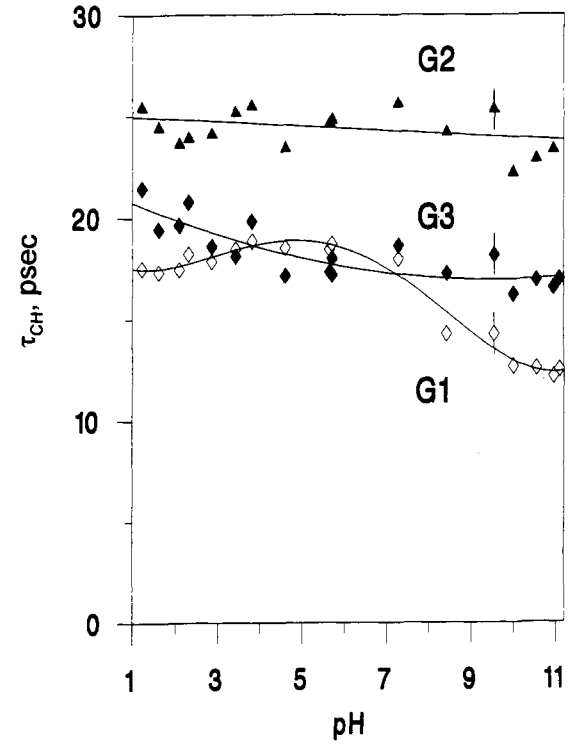

FIGURE 3: Titration curves for autocorrelation times, τ_{CH}, of the methylene groups in triglycine at 303 K. Peptide concentration is 25 mg/mL. These measurements have been done for ^{13}C nonenriched peptide. Experimental reproducibility is indicated by error bars shown for a few data points.

pH dependence is found for G3, where E_{CH} varies about 20% between pH 2.2 and pH 10.7.

Although cross-correlation times, τ_{HCH}, are rather small at all glycine positions under the conditions studied, significant temperature dependencies are noted in Figure 5 for G2 and G3 τ_{HCH}/τ_{CH} ratios (magnitude and sign), which are characteristic of methylene group rotational anisotropy (Daragan & Mayo, 1992). These results are consistent with previous findings on a hexadecapeptide where τ_{CH} and τ_{HCH}/τ_{CH} for nonterminal glycines showed similar behavior (Daragan et al., 1993b). For G1, the temperature dependence in τ_{HCH}/τ_{CH} is minimal at best. This is in line with previous results characterizing rotational motions of glycine at the N-terminal position (Daragan et al., 1993a). pH also influences the ratio τ_{HCH}/τ_{CH}. For G1 and G3, the lowest values for this ratio are found at pH 2.2. For G3, pH 5.6 values are largest, while for G1, pH 10.7 values are largest.

As discussed earlier in this article, molecular rotational models are normally parameterized in terms of the correlation time, τ_o, for reorientation of the C_α–$C_{carbonyl}$ bond for G1 and for reorientation of the C_α–N bond for G3. For G2, the analysis is more involved and will be discussed later. For all glycines, however, τ_o values can be derived from auto- and cross-correlation times by using eq 32.

$$\tau_o = 3(\tau_{CH} + 2\tau_{HCH}) \qquad (32)$$

This equation is strictly valid for the tetrahedral geometry of the CH_2 group. However, this should be a good approximation for glycine methylene geometry. τ_o values at 303 K are given in Table I. As with τ_{CH}, G3 gives a maximum τ_o value at pH 2.2, and for G1 τ_o is largest at pH 5.6. The temperature dependence in τ_o has been analyzed by using the Arrhenius equation, which yields linear plots of log τ_o versus the inverse temperature (K^{-1}). The resulting rotational energy barriers, E_o, are also given in Table I. For G1 and G3, E_o increases

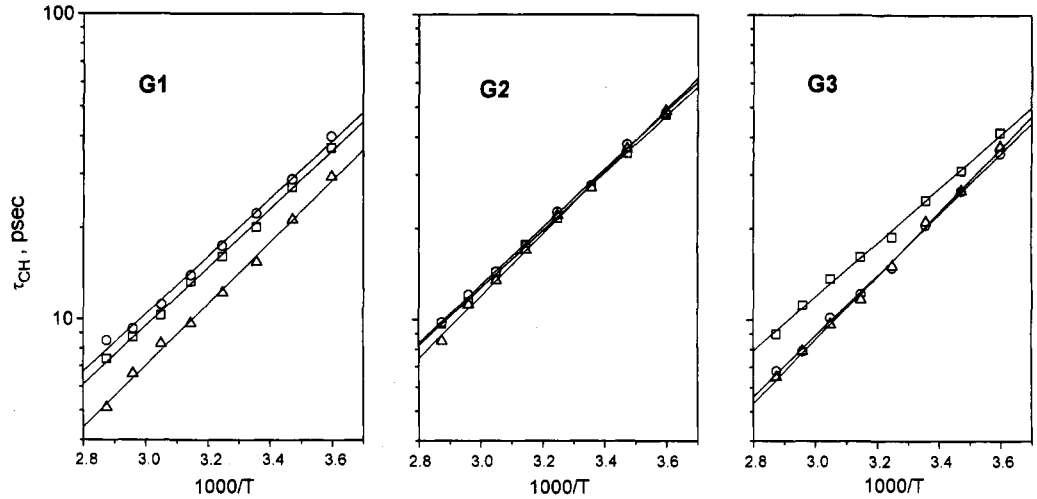

FIGURE 4: Temperature dependencies of correlation times, τ_{CH}, of the methylene groups in triglycine at different pH: □, pH 2.2; ○, pH 5.6; △, pH 10.7. Peptide concentration is 25 mg/mL.

Table I: Auto- and Cross-Correlation Times for GGG and GG Peptides at 303 K (ps) and Activation Energies (kcal/mol)[a]

glycine		pH 2.2	pH 5.6	pH 10.7
G1	τ_{CH}	18.1	20	14.2
G1	E_{CH}	4.26	4.33	4.64
G1	τ_o	50.1	58.9	49.5
G1	E_o	4.24	4.37	4.56
G1	τ_i	25.6	23.5	9.12
G1	E_i	5.45	5.26	6.27
G2	τ_{CH}	24.5	25.2	24.3
G2	E_{CH}	4.33	4.38	4.7
G2	τ_{HCH}	0.7	0.4	1
G2	τ_o	78.2	77.9	79.5
G2	E_o	3.8	3.48	4.06
G2	τ_i	23.9	25.7	21.9
G2	E_i	6.41	6.61	6.55
G3	τ_{CH}	22.8	17.7	17.8
G3	E_{CH}	4.06	4.57	4.8
G3	τ_o	66.4	58.7	55.4
G3	E_o	3.58	4.01	4.09
G3	τ_i	24.3	13.6	16.2
G3	E_i	6.22	6.33	6.56
G1 and G2 of GG	τ_o		49	
G1 and G2 of GG	E_o		3.3	
G1 of GG	τ_i		14	
G1 of GG	E_i		5.9	
G2 of GG	τ_i		18.1	
G2 of GG	E_i		6.52	

[a] τ_i are the correlation times of internal rotations for the restricted rotational diffusion model. τ_o are the correlation times of C_α–C and N–C_α for G1 and G2 (in GGG), respectively, and for G2 (in GGG) τ_o is determined from the restricted diffusion model.

with increasing pH, while for G2, E_o shows a minimum at pH 5.6.

The validity of eq 32 can be checked by measuring [^{13}C]-methylene relaxation parameters for diglycine. In this case, the correlation times for reorientation should be equal since the N–C_α bond of G2 is approximately parallel to the C_α–$C_{carbonyl}$ bond of G1. This is indeed what is observed. Results for τ_{CH} and τ_{HCH} are plotted in Figure 6. Due to the fact that τ_{CH} for G2 is larger than it is for G1 at any temperature and τ_{HCH} for G2 is more negative, it can be concluded that G1 is more mobile than G2. Note that the difference in mobility from diglycine G1 and G2 has also been detected by analyzing ^{2}H quadrupole relaxation data (Behr & Lehn, 1972). Calculation of τ_o using τ_{CH} and τ_{HCH} in eq 32 produces Figure 6, which gives essentially the same correlation times for G1 and G2.

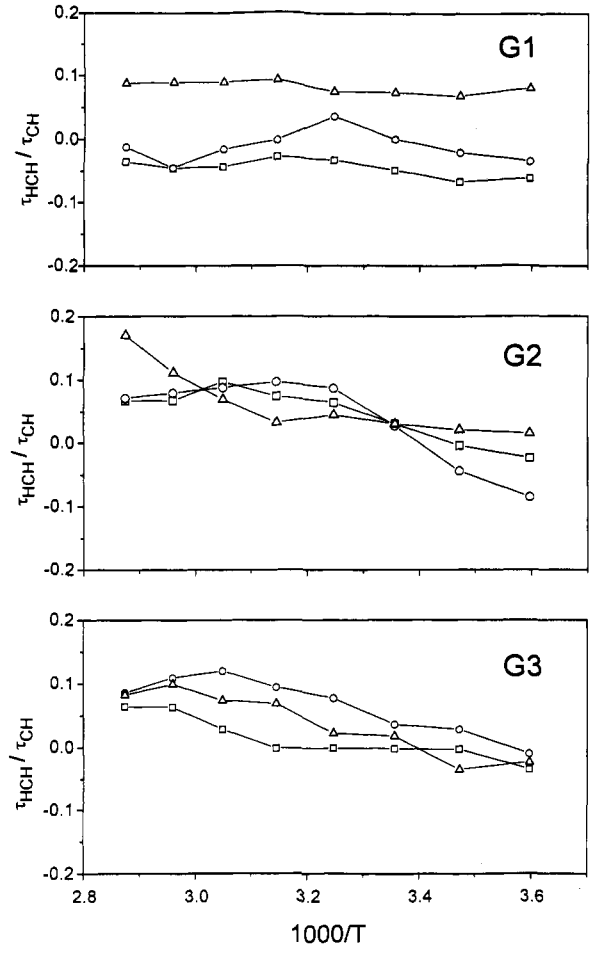

FIGURE 5: Temperature dependencies of cross-/autocorrelation times ratio τ_{HCH}/τ_{CH} of the methylene groups in triglycine at different pH values: □, pH 2.2; ○, pH 5.6; △, pH 10.7.

To check for possible triglycine aggregation, ^{13}C relaxation data were accumulated at peptide concentrations of 25 and 3.5 mg/mL. τ_{CH} values at pH 2.2, 5.6, and 10.7 are given in Figure 7. Some concentration effect is apparent since all correlation times are slightly smaller at the lower concentration. However, these can be explained generally by increased viscosity at the higher peptide concentration. The greatest change in τ_{CH} is noted for G3 at pH 2.2, although the relative change in τ_{CH} for G1 on going from pH 5.6 to 2.2 is larger at the lower peptide concentration.

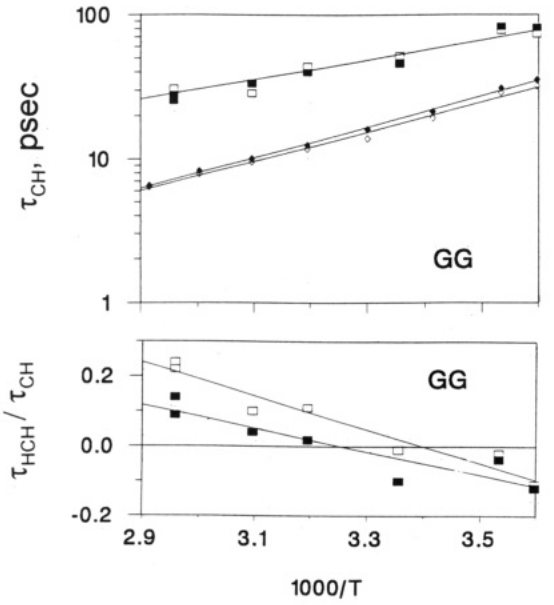

FIGURE 6: Temperature dependencies of autocorrelation times ratio τ_{CH} and cross-/autocorrelation times ratio τ_{HCH}/τ_{CH} of the methylene groups in diglycine at pH 6.0: □, N-terminal glycine; ■, C-terminus.

The effect of ionic strength on peptide mobility was addressed by the addition of 0.5 M NaCl to a triglycine sample (3.5 mg/mL). These results are also given in Figure 7. All τ_{CH} values increase with increasing ionic strength. For G1, however, the pH dependence in τ_{CH} is different, and no significant difference is observed on comparing data at pH 5.6 and 10.7.

Computational Modeling. Triglycine is the simplest peptide for computational modeling of intramolecular rotations. Energy profiles for φ and ψ rotations were calculated initially by using standard AMBER potential energy parameters in the DISCOVER program (Version 2.7.0, Biosym Technologies, Inc.). It should be mentioned that the AMBER force field assumes transferability of molecular electrostatic potential derived net atomic charges for all residues. Chipot et al. (1993) have shown that this transferability is nonexistent for a series of hydrocarbons. Glycine is evidently the most unique residue and perhaps would suffer most from this nontransferability. Although it may be argued that the use of standard AMBER potential energy parameters for glycine is questionable, here this approach provides a qualitative physical picture of intramolecular rotational energetics to be compared with those derived from experiment. In this respect, caution should be exercised in interpreting these AMBER-based energy calculations.

Energy minimization (conjugate gradient method) provided an equilibrium conformation of triglycine (*in vacuo*) with φ and ψ values as follows: $\psi_1 = 98.3°$, $\varphi_2 = 179.0°$, $\psi_2 = 97.6°$, and $\varphi_3 = 179.3°$. Bond rotations around individual glycine φ and ψ bonds were then incremented (5° increments), yielding the results shown in Figure 8. ψ rotations gave two well-defined minima separated by a rotational energy barrier of 2–2.2 kcal/mol and with a separation between the minima of 180°. For φ rotations, three minima resulted—one with the lowest potential at 180° and two with higher minima separated by 180°. These calculations were done *in vacuo* without taking into account electrostatic interactions. When electrostatic interactions (dielectric constant $\epsilon = 80$) were included in the calculations, equilibrium values for φ and ψ remained unchanged within about 1° and changes in the rotational energy profiles varied by less than 0.1 kcal/mol. This suggests that all changes observed in relaxation behavior at different pH values are the result of intermolecular water–peptide interactions.

Molecular dynamics calculations were then performed to investigate which internal rotations in triglycine are more favored. This approach is useful in analyzing the nature of various bond rotations and rotational restraints, which can be compared with those derived from mathematical model calculations. Simulations were performed *in vacuo* at 280 and 370 K, using the DISCOVER program. Each simulation was run with 3×10^6 steps, with time incremented in units

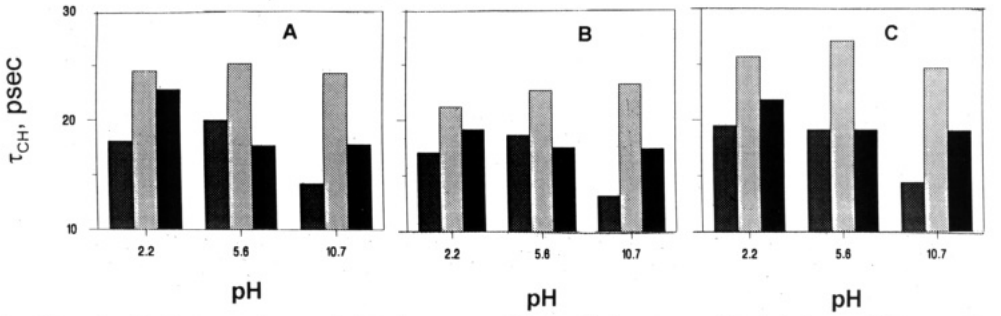

FIGURE 7: Concentration and salt effects on the correlation times τ_{CH} of the methylene groups in triglycine at different pH values. (A) Data for peptide concentration of 25 mg/mL. (B) Data for peptide concentration of 3.5 mg/mL. (C) Data for a peptide concentration of 3.5 mg/mL and a concentration of NaCl of 35 mg/mL. The left, middle, and right rectangles at each pH inside a panel are the correlation times for G1, G2, and G3, respectively.

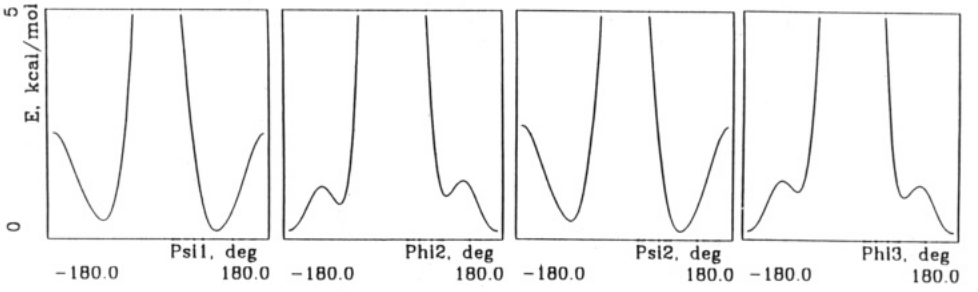

FIGURE 8: Energy profiles for φ and ψ rotations in triglycine *in vacuo*, calculated by using the DISCOVER program. All calculations were started from an equilibrium conformation with φ and ψ values of $\psi_1 = 98.3°$, $\varphi_2 = 179.0°$, $\psi_2 = 97.6°$, and $\varphi_3 = 179.3°$.

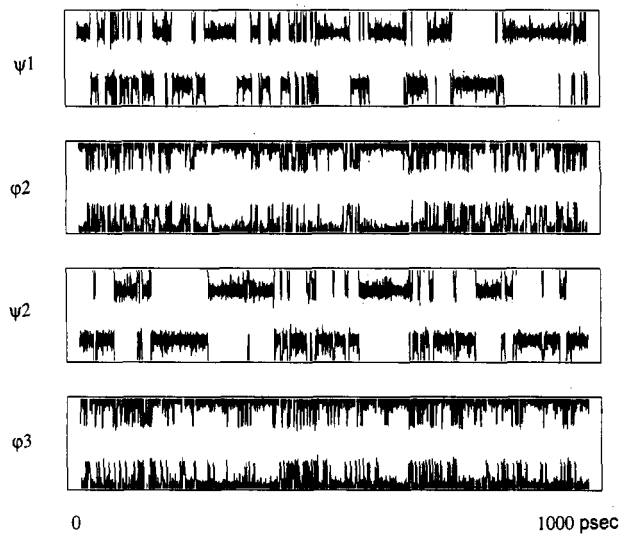

FIGURE 9: Time dependence of triglycine dihedral angle (ψ_1, φ_2, ψ_2, and φ_3) fluctuations taken from molecular dynamics simulations *in vacuo* (280 K) by using AMBER potentials. A 1000-ps run (one-third of the total run) with a sampling period of 0.1 ps is shown. *y*-axes on each graph vary from −180° to 180°.

of 10^{-15} s. Molecular files were recorded every 100 steps. Therefore, the results represent 3-ns simulations. This time scale provides sufficient statistics for calculating correlation function decays up to about 100 ps. These can then be compared with ^{13}C relaxation-derived correlation times.

The results shown in Figure 9 exemplify φ and ψ dihedral angle fluctuational time dependencies. For ψ_1 and ψ_2, internal rotations are best described as rotational jumps and oscillations within potential wells, whereas for φ_2 and φ_3, rotations are best described as quasi-oscillations within a potential well with jumps between two smaller, higher energy minima. Relative to the 280 K simulation, the 370 K simulation demonstrated similar types of internal rotations, albeit at higher transition frequencies.

If one defines γ and γ_{av} as the angle of internal rotation and its average, respectively, then the correlation function for each angle, $\Gamma(t)$, can be calculated by

$$\Gamma(t) = \langle \Delta\gamma(t_o + t)\Delta\gamma(t_o) \rangle \qquad (33)$$

where $\Delta\gamma = \gamma - \gamma_{av}$, and $\langle\ \rangle$ is the average over t_o. Results are displayed in Figure 10 (top). For φ and ψ, $\Gamma(t)$ behaves differently, decaying more rapidly with damped oscillations for φ rotations, but decaying more slowly in about 100 ps with far less frequent ψ rotational oscillations. For (φ,ψ) cross-correlation, i.e., $\Gamma'(t) = \langle \Delta\gamma(t_o + t)\Delta\gamma'(t_o) \rangle$, $\Gamma'(t)$ is negative, and for (ψ,φ) cross-correlation, $\Gamma'(t)$ is positive (Figure 10, middle). γ' defines an internal rotational angle that is different from γ. For each cross-correlation function, an initial decay spike is noted at short times. This apparently corresponds to oscillations in the φ autocorrelation function shown in Figure 10 (top). At higher temperatures, as one might expect, these cross-correlations become less pronounced.

Short-time molecular dynamics simulations (100 ps) of triglycine in water have been performed as well. Although statistics are rather poor, amplitudes of restricted rotations within the potential wells are more attenuated than those observed *in vacuo*, and oscillations in the autocorrelation

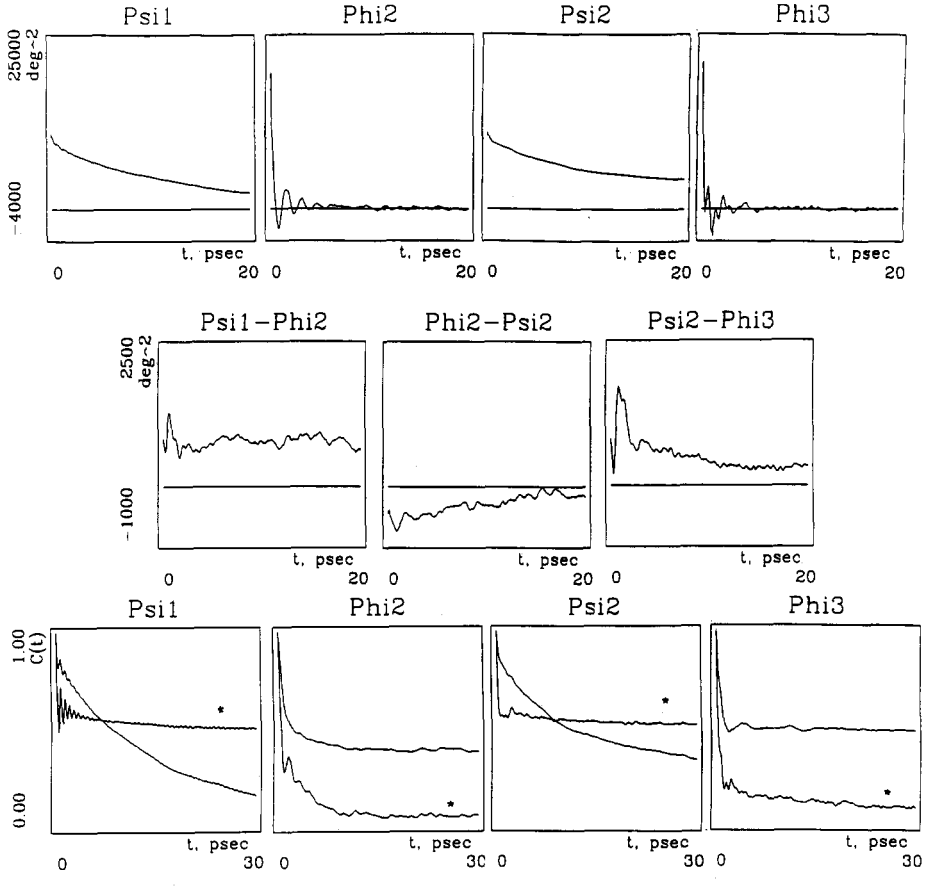

FIGURE 10: Auto- and cross-correlation functions for the ψ_1, φ_2, ψ_2, and φ_3 dihedral angles in triglycine from molecular dynamics simulations *in vacuo* (280 K). The top row shows the correlation functions, $\Gamma(t) = \langle \Delta\gamma(t_o + t)\Delta\gamma(t_o) \rangle$ (see text), where γ is one of the dihedral angles mentioned above. The second row shows the cross-correlation functions, $\Gamma'(t) = \langle \Delta\gamma(t_o + t)\Delta\gamma'(t_o) \rangle$. The third row shows the autocorrelation functions, $\Phi_m(t) = \langle \cos(m(\gamma(t) - \gamma(0))) \rangle$ for $m = 1$ (starred curves) and for $m = 2$. The axis labeled $C(t)$ stands for the cosine correlation function defined in the text.

functions are not as pronounced. Cross-correlation functions are noisy, although the difference (greater than 1 order of magnitude) in the behavior of $\Gamma(t)$ for φ and ψ rotations still exists.

To compare data on internal rotations derived from molecular dynamics simulations and model analyses of NMR relaxation experiments, the "cosine" correlation function, $Re(\Phi_m(t)) = Re(\langle \exp m_i(\gamma(t) - \gamma(0))\rangle) = \langle \cos(m(\gamma(t) - \gamma(0)))\rangle$, which is the real part of the internal rotation correlation function, has been calculated for all φ and ψ rotations (Figure 10, bottom). For ψ rotations with two potential wells, $Re(\Phi_2(t))$ decays in a few picoseconds, while $Re(\Phi_1(t))$ exhibits a much longer decay phase of tens of picoseconds. For φ rotations, $Re(\Phi_m(t))$ values decay in about 5 ps. The absolute value to which these functions decay depends on m and the number of bonds. We have also calculated the cross-correlation function, $Re(\langle \exp(m_i(\gamma(t) - \gamma'(t)))\rangle)$, where γ and γ' are φ or ψ angles. Such cross-correlations are insignificant with respect to autocorrelation functions. The choice of which rotational model best fits the relaxation data and gives the most meaningful physical picture in terms of the dynamics simulations and rotational energy profiles is discussed in the following section.

ANALYSIS AND DISCUSSION

Mobility of Nonterminal Triglycine Residue G2. Since the G3 N–C_α and the G1 C_α–C bonds are approximately parallel to the G2 C_α–C and N–C_α bonds, respectively, four correlation times can be determined for the G2 methylene group: three autocorrelation times, τ_{CH}, τ_{CC}, and τ_{NC}, and one cross-correlation time, τ_{HCH}. Table II shows that the values of τ_{CC} and τ_{NC} at 303 K are nearly equal for the zwitterionic form of the tripeptide. However, at low and high pH values, τ_{CC} is somewhat larger than τ_{NC}. At all pH values, τ_{CC} and τ_{NC} are about twice as large as τ_{CH}, and τ_{HCH} remains positive. These results indicate relatively large rotational anisotropy for the G2 methylene group.

Initially, ^{13}C relaxation data for G2 were analyzed by using the model of anisotropic unrestricted rotational diffusion (Huntress, 1968). Symmetric top motion presents the simplest anisotropic rotational model. Here, components of the rotational diffusion tensor are related as $D_{xx} = D_{yy} \neq D_{zz}$, and τ_{ab} defines the rotational correlation time (if $\mathbf{a} \neq \mathbf{b}$ we have the cross-correlation time):

$$\tau_{ab} = [a^0_{ab}/(6D_{xx})] + [a^1_{ab}/(5D_{xx} + D_{zz})] + [a^2_{ab}/(2D_{xx} + 4D_{zz})] \quad (34)$$

where

$$a^0_{ab} = 0.25(3z_a - 1)(3z_b - 1)$$

$$a^1_{ab} = 3z_a z_b(x_a x_b + y_a y_b)$$

$$a^2_{ab} = (^3/_4)((x_a x_b + y_a y_b)^2 - (x_a y_b - y_a x_b)^2)$$

x, y, and z are unit vectors for bonds **a** and **b** in the molecular frame, where the rotational diffusion tensor is diagonalized. Let us define the molecular frame for G2 where the z-axis bisects the HCH angle; the x-axis is perpendicular to the NCC plane, and the y-axis is perpendicular to the x- and z-axes. The superscript o denotes coordinates in this frame. Two rotations are needed to transform x^o, y^o, and z^o to x, y, and z: the first rotation is about the z-axis through an angle α, and the second rotation is about the new x-axis through the angle β. The coordinate transformation is defined as

$$x = \cos\alpha\, x^o + \sin\alpha\, y^o$$

$$y = -\cos\beta \sin\alpha\, x^o + \cos\beta \cos\alpha\, y^o + \sin\beta\, z^o \quad (35)$$

$$z = \sin\beta \sin\alpha\, x^o - \sin\beta \cos\alpha\, y^o + \cos\beta\, z^o$$

Using these equations, τ_{CH}, τ_{CC}, τ_{NC}, and τ_{HCH} can be fit to obtain α, β, D_{xx}, and D_{zz}. In Table II, it is apparent that the z-axis of the rotational diffusion tensor lies in the CCN plane, close to the C_α–C bond. Calculated correlation times agree rather poorly with the experimentally determined values. In particular, calculated τ_{HCH}/τ_{CH} values are 3–4 times larger at pH 2.2 and pH 10.7. This suggests that other rotations, probably more restricted ones, contribute to G2 ^{13}C relaxation.

For the model of restricted rotational diffusion (see the theoretical section), it has been assumed that the axis of internal restricted rotation makes an angle β with the z-axis, as described above. In order to reduce fitting errors, the value of γ was fixed at 90° from rotational energy calculations, and the same four correlation times were then fit to give model parameters τ_o, τ_i, and β as listed in Table III. The error in determining β for fixed values of γ is much less than that for the previous model (by about 2°), and it can be concluded that the angular deviation in the G2 C_α–C bond axis of fastest rotation (angle β) is 30° at high pH, 35° at the middle pH, and 20° at low pH. Although τ_o and β agree well with values of $^1/_6 D_{xx}$ and β derived from the model of unrestricted rotational diffusion, agreement with experimentally determined correlation times remains poor.

On comparison of these values with those of τ_i derived from the restricted rotational diffusion model, where the angle β is fixed and the direction of internal rotation coincides with the C_α–C bond (see Table I), this τ_i value is highly underestimated, while τ_o is somewhat overestimated. For both models discussed so far, calculated correlation times show

Table II: Results of Fitting Procedure for the G2 Glycine of the GGG Peptide for the Model of Unrestricted Symmetric Top Rotational Diffusion[a]

pH	τ_{CH}	τ_{CC}	τ_{NC}	τ_{HCH}/τ_{CH}	α	β	D_{xx}	D_{zz}	error
2.2	31.1	54.4	37.6	0.12	0	−100	2.55	11.5	0.24
	24.5*	66.4*	50*	0.03*					
5.6	31.9	46.0	46.3	0.12	0	−90	2.57	10.6	0.24
	25.2*	58.7*	58.9*	0.14*					
10.7	29.9	46.4	40.6	0.13	0	−100	2.72	11.5	0.2
	24.3*	55.4*	49.5*	0.04*					

[a] All correlation times are in ps, diffusion coefficient is in 10^9 s^{-1}, and angles are in degrres. Starred values of the correlation times are the experimental values, and others are the result of the fitting procedure. Error column gives the average square deviation of experimental correlation time values from their "best model describing" values. Standard errors in the fitting procedure are approximately 2° for α, 30° for β, and 0.1 × 10^9 s^{-1} for diffusion coefficients.

Table III: Results of the Fitting Procedure for the G2 Glycine of the GGG Peptide for the Model of Restricted Rotational Diffusion[a]

pH	τ_{CH}	τ_{CC}	τ_{CN}	τ_{HCH}/τ_{CH}	β	τ_o	τ_i	error
2.2	29.3	48.0	41.5	0.12	−95.4	60	65	0.18
	24.5*	66.4*	50*	0.03*				
5.6	31.5	47.3	47.7	0.11	−90.2	64	72	0.22
	25.2*	58.7*	58.9*	0.14*				
10.7	30.3	57.8	38.2	0.11	−105	65	58	0.2
	24.3*	55.4*	49.5*	0.04*				

[a] All correlation times are in ps, and angles are in degrees. Starred values of the correlation times are the experimental values, and others are the result of the fitting procedure. Errors of the fitting procedure are 2° for β and 1 ps for correlation times.

significant deviations from experimentally determined ones. Even the Lipari and Szabo model-free approach (Lipari & Szabo, 1982a,b) cannot describe adequately these experimental data, especially the value of τ_{HCH}/τ_{CH}. This means that new models are needed for a more accurate description of backbone motions of nonterminal residues.

Mobility of Terminal Residues in Di- and Triglycine. For N- and C-terminal glycine residues, two correlation times are available: τ_{CH} and τ_{HCH}. The simplest model of restricted diffusion has three parameters: overall correlation time τ_o, internal motional correlation time τ_i, and the angle 2γ over which the rotational motion occurs. The value $2\gamma = 180°$ has been taken from rotational energy calculations discussed earlier. It has also been assumed that this value is independent of temperature and pH changes. For N- and C-terminal glycines, internal rotations about C_α–C and N–C_α bonds, respectively, will be considered. Results of this model analysis for diglycine and triglycine are listed in Table I. For comparison, τ_i and the corresponding energy barrier E_i have been calculated for the triglycine G2 position.

E_i for C-terminal glycine in GG and GGG is on the order of 0.3–0.8 kcal/mol larger than that for the N-terminal glycine position, with the smallest difference being noted at pH 10.7. This is consistent with the C-terminal carboxylate being bulkier and being able to form more hydrogen bonds with water than the N-terminal amine. On titration to above the carboxylic acid pK_a of 3.4, i.e., pH 5.6 and pH 10.7 data, the change in oxygen hybridization from sp^2 to sp^3 results in a reduction from 5 to 4 hydrogen bonds. In this respect, a significant change in τ_i with pH is noted, although the energetic changes are not as pronounced. On passing through the amine pK_a value of 8.4, N-terminal glycine changes in both τ_i and E_i are rather significant. In particular, τ_i decreases by more than 2-fold. For the uncharged N-terminus, it seems that the conformational change increases the internal potential energy barrier, and the reduction in electrostatic potential generates increased mobility. For both N- and C-termini, therefore, a reduction in electrostatic interactions apparently favors increased internal rotational mobility.

Jump Model Analysis of Terminal Glycine Rotational Mobilities. For triglycine, there is an apparent contradiction between NMR relaxation data and potential energy calculations. Experimentally, G1 and G3 mobilities are similar and should be determined mainly by ψ_1 and φ_3 rotations, respectively. However, energy profiles for ψ_1 and φ_3 rotations appear to be quite different (see Figure 8). The internal rotational correlation function $\Phi_m(t)$ also shows different behavior for ψ_1 and φ_3 rotations (Figure 10). To explain this apparent contradiction, one might analyze the experimental results by considering an internal rotational jump model where rotational fluctuations within potential wells are taken into account. Alternatively, a multiple rotation model might be considered. For diglycine, however, similar relaxation behavior for N- and C-terminal glycines exists, and here there are no multiple rotations. This means that initially one should analyze the relaxation data by using the jump model with rotational fluctuations. As a first approximation in this analysis, cross-correlations of various internal rotations have been neglected as suggested by calculations of $Re(\langle \exp(m_i(\gamma(t) - \gamma'(0))))\rangle)$. This assumes that, for such short peptides, correlated or concerted motions are not so important to ^{13}C relaxation.

For G1 and G3, values of the correlation time, τ_o, for reorientation of the C_α–C and N–C_α bonds, respectively, have been given. To analyze the internal rotational characteristics, only one additional independent experimental parameter τ_{HCH}/τ_{CH}, for example, is needed. From eq 28, one can write a general equation for this ratio:

$$\tau_{HCH}/\tau_{CH} = (-^1/_3 + x)/(1 - 2x) \quad (36)$$

where for any model of internal rotation, $x = C(\gamma)\tau_o/(\tau_o + \tau_i)$. From our experimental data, $|\tau_{HCH}/\tau_{CH}| < 0.1$ for both G1 and G3, and from eq 36, one can estimate that $0.29 < x < 0.37$.

For G1 rotations, calculated rotational energy profiles indicate that a two-state jump model is appropriate. For ψ_1 rotations, $C(\gamma)$ and the ratio $\xi = \tau_o/(\tau_o + \tau_i)$ (when $\tau_o \gg \tau_i$) have a weak temeprature dependence at best. Therefore, as observed in Figure 5, the ratio τ_{HCH}/τ_{CH} is not expected to show a strong temperature dependence. On the other hand, for a two-state jump model, $C(\gamma = 90°) \approx 0.15$. This value, however, is not large enough to produce the experimentally observed positive sign of τ_{HCH}/τ_{CH} at any value of ξ. For this model with $\gamma = 90°$, the correlation function $\Phi_m(t)$ (see eq 24) yields $\Phi_1(t) = \exp(-2Wt)$ and $\Phi_2(t) = 1$. From molecular dynamics simulations (Figures 9 and 10), one can see that a relatively fast process, i.e., 1–2 ps time scale, substantially alters the correlations. It seems obvious that one should consider rotational fluctuations within potential wells and their influence on these correlation times. Note that Clore et al. (1990a,b) also had to consider similar fast, restricted rotational motions to adequately describe ^{15}N NMR relaxation data in proteins.

To a good approximation, one can write the correlation function $\Phi_m(t)$, where jumps between and rotational fluctuations within potential wells are taken into account:

$$\Phi_m(t) = 1 - C_m - C_m^f + C_m \exp(-t/\tau_i) + C_m^f \exp(-t/\tau_f) \quad (37)$$

where τ_i is the correlation time of the rotational fluctuations, and C_m^f is a function of the amplitude δ of these fluctuations. $C_o^f = 0$. Equation 37 can be obtained, for example, by considering "double" rotations around the same axis where the transformation matrix (see eq 12) $B_{m_1,m}(\beta) = B_{m_1,m}(0) = \delta_{m_1,m}$ and $C_m C_m^f \ll C_m$ and C_m^f. Usually $\tau_f \ll \tau_i$, and one can write

$$x = C^f(\delta) + C(\gamma)\tau_o/(\tau_o + \tau_i) \quad (38)$$

where $C^f(\delta) = (^4/_{27})(C_1^f + 2C_2^f)$. $C^f(\delta)$ does not depend significantly on temperature, as reflected in eqs 36 and 38 which produce a small temperature dependence in the ratio τ_{HCH}/τ_{CH} for G1. Equation 37 can describe the molecular dynamics data for $\Phi_m(t)$. After considering the short-time behavior of $\Phi_m(t)$ (Figure 10), one can estimate that $C_1^f/C_2^f \approx 0.4$. If we apply the restricted diffusion model to describe rotational fluctuations, the amplitude of rotational fluctuations within the potential wells is $2\delta = 126°$. From the simplified random walk model, one can estimate $2\delta = 149°$ for $2W^+/W^- = 0$ and $2\delta = 172°$ for $2W^+/W^- = 0.2$. These 2δ values are larger than those estimated from the time dependence of $\psi_1(t)$ (see Figure 9). By applying the two-state jump model to describe these internal rotational fluctuations, $C_1^f/C_2^f = 0.25/\cos^2\delta$ (eq 24) and for $C_1^f/C_2^f = 0.4$, $2\delta = 75°$. This agrees well with the result derived from the time dependence of $\psi_1(t)$. The relative success of this model is based on the quasi-periodical character of the rotational fluctuations occurring within the potential well. The two-state jump model can approximate such motions.

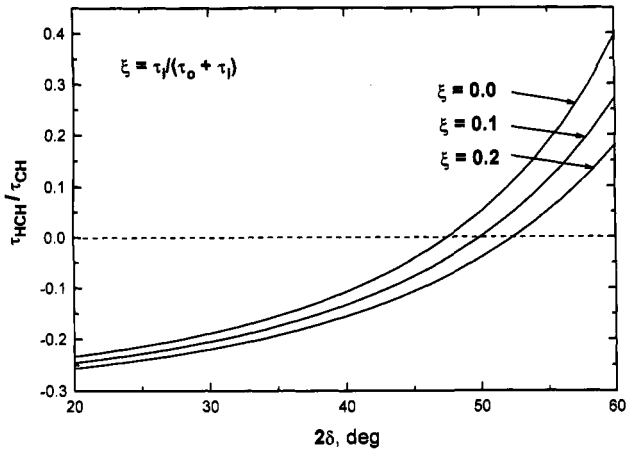

FIGURE 11: For different τ_i/τ_o ratios, calculated cross-/autocorrelation times ratio τ_{HCH}/τ_{CH} for a two-state jump model with rotational fluctuations within the potential wells. τ_i and τ_o are the correlation times of rotational jump motion and tumbling, respectively. The x-axis in this plot gives the double amplitude of rotational fluctuations within the potential wells.

For different values of τ_i/τ_o, calculation of the ratio τ_{HCH}/τ_{CH} versus 2δ is given in Figure 11. Apparently, there is no significant dependence of $\tau_{HCH}/\tau_i/\tau_o$ over this limited range, and these calculations help explain why the G1 τ_{HCH}/τ_{CH} temperature dependence is so weak. Under the assumption that $\tau_i/\tau_o \ll 1$, 2δ is equal to 45° at low or neutral pH, and $2\delta = 51°$ at high pH. Reduction of τ_i increases the value of τ_{HCH}/τ_{CH}. Therefore, at pH 10.7, neutralization of the N-terminal amine promotes increased mobility at the G1 methylene group. This induces increased rotational fluctuation amplitudes of up to 6° and reduces internal correlation times.

Calculation of rotational energy profiles for diglycine shows that ψ_1 rotation can also be described by rotational jumps between two states separated by 180°. As can be seen in Figure 5, the ratio τ_{HCH}/τ_{CH} does depend on temperature. On going from 278 to 343 K, the value of x (see eq 38) for G1 in diglycine varies from 0.30 to 0.36. This indicates that the ratio τ_i/τ_o for GG is not small, as was assumed for GGG. Note that for GG, as well as for GGG, one cannot describe the NMR relaxation data without assuming the presence of fast rotational fluctuations within potential wells.

From molecular dynamics simulations, it appears that for C-terminal glycines, both internal rotational correlation times, τ_i and $\tau_f \ll \tau_o$. This significantly simplifies the analysis of NMR relaxation data for GG and GGG. The rotational energy profile for φ_3 indicates that a three-state rotational jump model with $\gamma = 90°$ is best at describing the experimental data. For this case, one can write $C(\gamma) = ({}^{80}/_{27})W_0/W_1$ (see notation in the theoretical section). The rotational fluctuations within the potential well can be described as mentioned earlier. For triglycine G3 rotations, one can write

$$x = C^f(\delta) + ({}^{80}/_{27})W_0/W_1 \qquad (39)$$

where $W_0/W_1 = \exp(-\Delta E/RT)$, and ΔE is the energy difference between major and minor minima. From eqs 36 and 39, it is apparent that the temperature dependence in τ_{HCH}/τ_{CH} results from the temperature dependence in W_0/W_1. ΔE and $C^f(\delta)$ can be determined from our experimental data. To derive δ, it has been assumed that rotational fluctuations can be described by the two-state jump model. Fitted values of ΔE, $C^f(\delta)$, and δ for C-terminal glycines in tri- and diglycine are given in Table IV. ΔE substantially exceeds the calculated value *in vacuo* by 1 kcal/mol. C-terminal carboxylate interactions with water molecules probably modify the energy profile for φ_3 rotations (φ_2 for GG). The minor "side" minima, therefore, become deeper, causing W_0/W_1 to increase. Since fitting errors for ΔE are about 0.3–0.4 kcal/mol, pH evidently does not disturb ΔE substantially, whereas $C^f(\delta)$ varies by 10% with pH. At low pH, G3 in GGG has a relatively high ΔE value and low $C^f(\delta)$ and δ values, indicating relatively slow internal rotations. It should be mentioned, however, that the effect of pH on internal mobility is more pronounced at the N-terminal glycine.

Table IV: Parameters of Internal Rotations of C-Terminal Glycines in the GG and GGG Peptides[a]

peptide	glycine	pH	ΔE	δ	C^f	error
GGG	G3	2.2	2.7	34	0.31	0.02
GGG	G3	5.6	3.0	34	0.33	0.03
GGG	G3	10.7	2.9	37	0.31	0.01
GG	G2	6.0	2.2	29	0.25	0.02

[a] ΔE is in kcal/mol; δ is in degrees.

It was surprising that δ for G2 in diglycine (see Table IV) is less than δ for G3 in triglycine. Rotational energy profiles for both φ rotations (φ_3 for GGG and φ_2 for GG) are identical, indicating similar behavior for internal rotational fluctuations at these terminal positions. To understand this contradiction, one should remember that, in the derivation of the present equations, internal rotation and overall tumbling were assumed to be independent. Presumably, this assumption is more valid for triglycine. The C-terminal carboxylate can form several hydrogen bonds with water molecules, which in turn help anchor it with respect to the remainder of the peptide. Such an effect will be larger for the shorter dipeptide. Rotation of the C-terminal glycine about the N–C_α bond causes N-terminal rotation about this axis to occur in the opposite direction. This in turn attenuates reorientation of the CH glycine vectors with respect to the laboratory frame and apparently reduces δ. In our opinion, this effect should be important for conformational fluctuations (small fluctuations in φ and ψ dihedral angles) in proteins and should be taken into account in the analysis of relaxation data.

Finally, one can conclude that rotational fluctuations within potential wells are rather important to the interpretation of NMR relaxation data. Dipolar cross-correlation spectral densities (cross-correlation times for small molecules) are good indicators for assaying these fluctuations. In polypeptides and proteins, such fluctuations are apparently the main mechanism for internal rotational mobility. These fluctuations can be regarded as searching out paths along which conformational transitions may occur. They serve as the "lubricant" (Karplus, 1986) which makes possible larger scale displacements on a physiological time scale. In this respect, it may be possible to extrapolate from short time scale fluctuations to longer time scale, more biologically important, protein internal motions.

ACKNOWLEDGMENT

Dr. Marek Kloczewiak is gratefully acknowledged for preparing isotopically enriched triglycine samples.

REFERENCES

Atherton, E., & Sheppard, R. C. (1989) in *Solid phase peptide synthesis: A practical approach*, IRL Press, Oxford, England.

Bain, A. D., & Lynden-Bell, R. M. (1975) *Mol. Phys. 30*, 325–356.

Behr, J. P., & Lehn, J. M. (1972) *J. Chem. Soc., Perkin Trans. 2* 1488–1492.

Chipot, C., Angyan, J. G., Ferency, G. G., & Scheraga, H. J. (1993) *J. Phys. Chem. 97*, 6628–6636.
Clore, G. M., Szabo, A., Bax, A., Kay, L. E., Driscoll, P. C., & Gronenborn, A. M. (1990a) *J. Am. Chem. Soc. 112*, 4989–4991.
Clore, G. M., L. E., Driscoll, P. C., Wingfield, P. T., & Gronenborn, A. M. (1990b) *Biochemistry 29*, 7387–7401.
Daragan, V. A., & Mayo, K. H. (1992) *J. Am. Chem. Soc. 114*, 4326–4331.
Daragan, V. A., & Mayo, K. H. (1993) *Chem. Phys. Lett. 206*, 393–400.
Daragan, V. A., Khazanovich, T. N., & Stepanyants, A. U. (1974) *Chem. Phys. Lett. 26*, 89–92.
Daragan, V. A., Kloczewiak, M. A., & Mayo, K. H. (1993a) *Biochemistry (in press)*.
Daragan, V. A., Ilyina, E. E., & Mayo, K. H. (1993b) *Biopolymers 33*, 521–533.
Edholm, O., & Blomberg, C. (1979) *Chem. Phys. 42*, 449–464.
Huntrees, W. T., Jr. (1968) *J. Chem. Phys. 48*, 3524–3533.
Karplus, M. (1986) *Methods Enzymol. 131*, 283–307.
Lipari, G., & Szabo, A. (1980) *Biophys. J. 30*, 489–506.
Lipari, G., & Szabo, A. (1981) *J. Chem. Phys. 75*, 2971–2976.
Lipari, G., & Szabo, A. (1982a) *J. Am. Chem. Soc. 104*, 4546–4559.
Lipari, G., & Szabo, A. (1982b) *J. Am. Chem. Soc. 104*, 4559–4570.
London, R. E. (1980) in *Magnetic Resonance in Biology*, Vol. 1, pp 1–69, Wiley, New York.
London, R. E., & Avitable J. (1978) *J. Am. Chem. Soc. 100*, 7159–7165.
Newman, R. H. (1982) *J. Magn. Reson. 47*, 138–141.
Ribeiro, A. A., King, R., Restivo, C., & Jardetzky, O. (1980) *J. Am. Chem. Soc. 102*, 4040–4051.
Sack, R. A. (1957) *Proc. Phys. Soc. (London) B70*, 402–413.
Saitô, H., & Smith, C. P. (1973) *Arch. Biochem. Biophys. 158*, 154–163.
Saitô, H., & Smith, C. P. (1974) *Arch. Biochem. Biophys. 163*, 699–704.
Tsutsumi, A. (1979) *Mol. Phys. 37*, 111–127.
Wallach, D. J. (1967) *J. Chem. Phys. 47*, 5258–5268.
Werbelow, L. G., & Grant, D. M. (1975) *J. Chem. Phys. 63*, 544–556.
Werbelow, L. G., & Grant, D. M. (1977) *Adv. Magn. Reson. 9*, 189–301.
Witterbort, R. S., & Szabo, A. (1978) *J. Chem. Phys. 69*, 1722–1736.
Zatsepin, V. M. (1977) *Teor. Mat. Fiz. (USSR) 33*, 400–408.